Moiré Tuning of Spin Excitations: Individual Fe Atoms on $MoS_2/Au(111)$

Sergey Trishin,[1] Christian Lotze,[1] Nils Bogdanoff,[1] Felix von Oppen,[2] and Katharina J. Franke[1,*]

[1]*Fachbereich Physik, Freie Universität Berlin, 14195 Berlin, Germany*
[2]*Dahlem Center for Complex Quantum Systems and Fachbereich Physik, Freie Universität Berlin, 14195 Berlin, Germany*

Magnetic adatoms on properly designed surfaces constitute exquisite systems for addressing, control-ling, and manipulating single quantum spins. Here, we show that monolayers of MoS_2 on a Au(111) surface provide a versatile platform for controllably tuning the coupling between adatom spins and substrate electrons. Even for equivalent adsorption sites with respect to the atomic MoS_2 lattice, we observe that Fe adatoms exhibit behaviors ranging from pure spin excitations, characteristic of negligible exchange and dominant single-ion anisotropy, to a fully developed Kondo resonance, indicating strong exchange and negligible single-ion anisotropy. This tunability emerges from a moiré structure of MoS_2 on Au(111) in conjunction with pronounced many-body renormalizations. We also find striking spectral variations in the immediate vicinity of the Fe atoms, which we explain by quantum interference reflecting the formation of Fe-S hybrid states despite the nominally inert nature of the substrate. Our work establishes monolayer MoS_2 as a tuning layer for adjusting the quantum spin properties over an extraordinarily broad parameter range. The considerable variability can be exploited for quantum spin manipulations.

Individual magnetic atoms on surfaces hold substantial promise for manipulating and coherently controlling quantum spin states [1]. A prerequisite is that the spin states are protected against relaxation and decoherence due to their coupling to the substrate [2], while remaining addressable by tunneling currents. Placing adatoms directly on metallic substrates is problematic as the creation of electron-hole pairs and spin-spin scattering involving the conduction electrons provide pathways for rapid energy and angular momentum relaxation [2–5]. However, relaxation and decoherence can be efficiently suppressed while retaining addressability when using metallic substrates passivated by thin decoupling layers such as nitrides [6] or oxides [7–9].

While suppressing relaxation and decoherence, these substrates provide limited (if any) tunability of the funda-mental interactions governing the quantum spin dynamics. Here, we show that monolayers of MoS_2 on Au(111) provide exquisite control over these interactions while simultaneously acting as efficient decoupling layers. The dynamics of individual quantum spins is dominated by the exchange coupling between adatom spin and substrate electrons as well as the single-ion anisotropy. We find that even for nominally identical adsorption sites of Fe atoms with respect to the MoS_2 lattice, the ratio between these interactions can be tuned essentially at will as a result of the interplay of a moiré structure of MoS_2 on Au(111) with strong many-body renormalizations. This provides consid-erable added functionality to van der Waals interlayers for decoupling magnetic adsorbates from metallic substrates.

Previous work on the van der Waals materials hexa-gonal boron nitride [10,11] and graphene [12,13] had demonstrated extended lifetimes as well as coherence times of excited spin states. A strongly site-specific Kondo resonance of Co atoms could be induced on Ru(0001) covered by graphene, which partially detached due to periodic rippling [14]. A moiré structure of hexagonal boron nitride on Rh(111) exhibited small variations in the magnetic excitation energies of hydrogenated Co adatoms with adsorption site [11]. Monolayers of transition metal dichalcogenides have previously been used to decouple organic molecules from metal substrates [15,16].

Using scanning tunneling microscopy and spectroscopy at a temperature of 1.1 K, we systematically study the magnetic excitation spectra of individual Fe atoms on Au(111) covered by a monolayer of MoS_2. The MoS_2 islands were grown by depositing Mo atoms on a clean Au(111) surface and subsequent annealing to 800 K in H_2S gas at a pressure of $p = 10^{-5}$ mbar [17,18] before depositing a dilute amount of Fe atoms at < 10 K. We find that the moiré structure imposes dramatic variations of the exchange coupling between Fe adatoms and substrate, even for identical adsorption sites with respect to the atomic MoS_2 lattice. When probing directly above the Fe atoms, we observe almost pure inelastic spin excitations in the minima of the moiré structure. Away from the minima, an increase of the moiré-modulated density of states enhances the exchange coupling, culminating in a fully developed Kondo resonance for Fe atoms located at moiré maxima. This is complemented by pronounced local variations in the immediate vicinity of the Fe atom, which we trace to quantum interference involving a separate orbital.
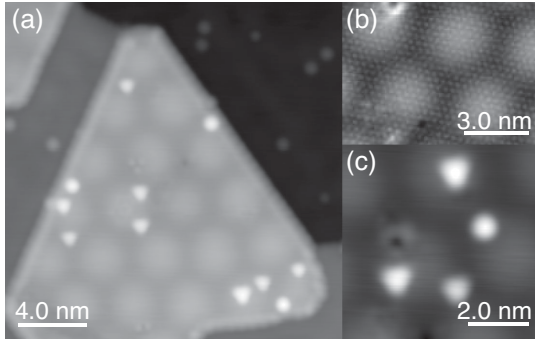
FIG. 1. (a) STM image of MoS_2 on Au(111) with a small number of iron atoms. ($V = 50$ mV, $I = 100$ pA). (b) Atomic-resolution topography of a clean MoS_2 island. ($V = 5$ mV, $I = 42$ nA). (c) Close-up of individual Fe atoms on a MoS_2 island. At low bias voltages, most atoms appear triangular. ($V = 50$ mV, $I = 100$ pA).

Figure 1(a) shows an STM image of a monolayer island of MoS_2 on Au(111) with a small coverage of Fe adatoms. The hexagonal corrugation within the MoS_2 island with a periodicity of ~3.3 nm reflects a moiré structure due to a lattice mismatch between the Au and S layers, causing a modulation of the electronic structure, see Supplemental Material [19] and Refs. [17,18,22]. An atomically resolved image of a clean MoS_2 area [Fig. 1(b)] shows the terminating S layer and resolves a minute amount of intrinsic point defects (see the upper and lower edge of the image). We focus on adatoms far from the defect sites to avoid any influence on the magnetic properties.

A close-up view of several Fe adatoms on a MoS_2 island is shown in Fig. 1(c). When scanned at low bias voltage,

most Fe adatoms appear as triangular shape, while a few atoms are imaged as round protrusions (see Supplemental Material [19]). All triangles point in the same direction relative to the underlying S lattice. The threefold symmetric shape indicates that these Fe atoms are located in equivalent sites of the MoS_2 lattice with partially filled crystal-field split d levels [23]. Density-functional-theory calculations (on free-standing MoS_2) suggest that the S-hollow sites with a Mo atom underneath are energetically favored [24,25].

To investigate the magnetic properties of the individual triangular-appearing Fe atoms, we recorded differential conductance (dI/dV) spectra of ~40 atoms. Figure 2 displays a characteristic set of spectra. We find dramatic variations of the spectral line shapes depending on the Fe adatom's position with respect to the moiré pattern. The Fe atom in Fig. 2(a) is located in a minimum of the moiré structure. Its dI/dV signal exhibits stepwise increases of intensity at ±2.7 mV. The Fe atom in Fig. 2(b) is shifted slightly off the minimum and shows a small overshoot of the differential conductance at positive bias voltages above the inelastic excitation threshold. This overshoot becomes more pronounced for Fe atoms located further from a moiré minimum [Figs. 2(c) and 2(d)]. Concomitantly, the steplike feature shifts to lower energies. Adatoms located close to a moiré maximum exhibit line shapes which resemble a Frota peak with an additional dip at the Fermi level [Fig. 2(e)]. Directly at the moiré maximum, the inelastic gap disappears and gives way to a fully developed asymmetric Frota peak [Fig. 2(f)].

To understand these spectroscopic characteristics of individual Fe atoms, we first discuss their electronic configuration. Consistent with the triangular shape of the electronic structure reflected in the STM images
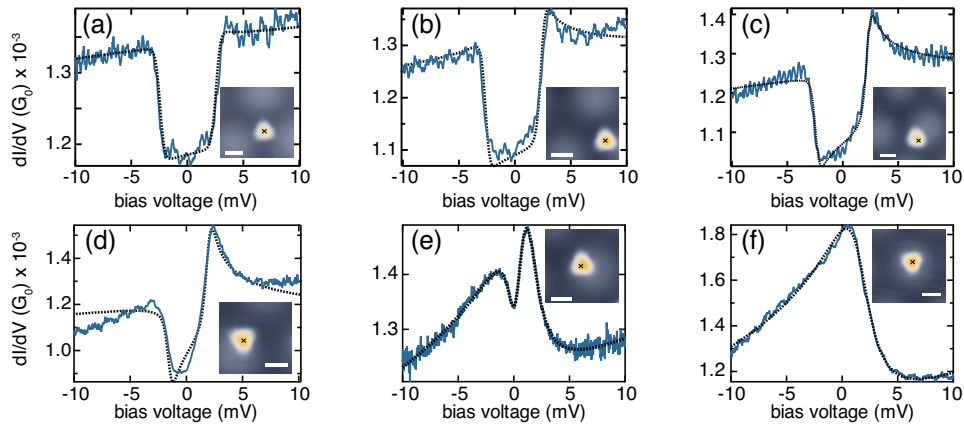

FIG. 2. dI/dV spectra at the center above Fe adatoms (blue) in different moiré environments as indicated by the STM topographies in the insets (scale bars are 1 nm, crosses mark the location of the spectra). The Fe atoms are located on islands with different orientations with respect to the Au(111) lattice [18]. Correspondingly, the triangles point in opposite directions. Fits are shown as black dashed lines. The spectrum in (a) can be reproduced by symmetric Fermi-Dirac functions. The spectra in (b)–(d) exhibit additional cusps on top of the inelastic steps. These spectra are fitted within a perturbative approach in the exchange interaction [26]. Spectrum (e) was fitted using a Frota line shape with an additional Lorentz peak. In (f), the spin excitation gap has closed, resulting in a fully developed Frota line shape. For fit parameters see Ref. [19]. Spectra recorded at $V = 10$ mV, $I = 1$ nA, lock-in frequency $f = 911$ Hz and modulation $V_{rms} = 50$ μV.

(see further discussion below), the hollow adsorption site imposes a trigonal-pyramidal crystal field which lifts the degeneracy of the d levels. Simple crystal field considerations suggest a splitting into two sets of doubly degenerate states, one of mostly d_{xz} and d_{yz} character and another of $d_{x^2-y^2}$ and d_{xy} character, as well as a high-lying nondegenerate state deriving from the d_{z^2} orbital. Depending on the ratio between the crystal field splitting and Hund's energy, filling these levels with six d electrons either leads to a spin state of $S = 2$ with a singly occupied d_{z^2} orbital, or to $S = 1$ with an empty d_{z^2} orbital [27].

Because of magnetocrystalline anisotropy, the spin $\hat{\mathbf{S}}$ prefers to align along a distinct direction even at zero magnetic field. This is described by the spin Hamiltonian $\hat{H} = D\hat{S}_z^2 + E(\hat{S}_x^2 - \hat{S}_y^2)$, where D is the axial and E the transverse magnetic anisotropy [6]. Inelastic spin excitations ($\Delta m = \pm 1$) lead to the opening of an inelastic tunneling channel and, thus, a stepwise increase of the junction conductance.

The dI/dV spectrum in Fig. 2(a) can indeed be well reproduced by a broadened Fermi-Dirac distribution function at ± 2.7 mV. Thus, the spectra probe magnetic atoms subject to a local crystal field and single-ion anisotropy characteristic of the adsorption site. The measured width $w = 0.45$ meV of the step is larger than the experimental broadening at $T = 1.1$ K, suggesting a lower bound of ~ 1 ps for the spin lifetime. Significantly broader steps are observed for Fe atoms in direct contact with a metal substrate [3,4,28,29]. This confirms that a single layer of MoS_2 acts as an efficient decoupling layer for the Fe atoms.

At the same time, the decoupling efficiency depends sensitively on the position of the Fe atom relative to the moiré lattice. As we observe line shapes ranging from inelastic steps to fully developed Kondo peaks, there must be variations in the magnitude of the coupling to the substrate. At and close to the minimum of the moiré structure [Figs. 2(a)–2(c)], the inelastic steps can be understood by considering the exchange coupling to the substrate perturbatively. To describe the conductance overshoot, one needs to go beyond lowest-order perturbation theory and include processes in the second-order Born approximation [26]. The asymmetry in the bias polarity can be reproduced when including potential scattering at the impurity in addition to the exchange coupling. Figures 2(a)–2(c) include corresponding fits [26]. These indicate that both the exchange coupling J and the potential scattering U increase as the adatom location moves off the moiré minimum [11,26]. In addition, there is a substantial reduction in the longitudinal anisotropy D.

For Fe atoms located further from the moiré minima, the pronounced changes in the line shape can no longer be captured within this perturbative framework. The transition to a fully developed Kondo line shape requires a strong-coupling approach and can be captured within a poor-person's scaling approach [30]. In the present case, one

should account for the longitudinal anisotropy as well as the higher impurity spin. Allowing for anisotropic exchange couplings $J_\perp$ and J_z and focusing on the simplest spin state $S = 1$ consistent with our experimental data, the scaling equations take the form [31]

$$\frac{dJ_z}{d\ell} = \frac{1}{1-\Delta}J_\perp^2, \tag{1}$$

$$\frac{dJ_\perp}{d\ell} = \frac{1}{2}\left(1 + \frac{1}{1+\Delta}\right)J_\perp J_z, \tag{2}$$

$$\frac{d\Delta}{d\ell} = \Delta - (J_z^2 - J_\perp^2)\ln 2. \tag{3}$$

Here, the exchange couplings are made dimensionless by means of the density of states ρ of the conduction electrons, $\rho J \to J$, the scaling variable ℓ parametrizes the bandwidth E_c, $\ell = \ln(E_{c0}/E_c)$, with initial bandwidth E_{c0}, and $\Delta = D/E_c$ measures the longitudinal anisotropy in units of the bandwidth.

As the adsorption site moves towards the moiré maximum, the associated change in the density of states increases the bare exchange couplings and hence the Kondo temperature. A fully developed Kondo peak is expected once the Kondo temperature exceeds the longitudinal anisotropy D. The scaling equations suggest that this effect is reinforced by the renormalization of D. For easy-axis anisotropy ($D > 0$ and $J_z > J_\perp$) as well as easy-plane anisotropy ($D < 0$ and $J_z < J_\perp$), the anisotropy D is reduced in magnitude during renormalization [see the second term on the right-hand side of Eq. (3)]. This further favors the crossover to fully developed Kondo correlations and is consistent with the observation that the threshold voltage of spin excitations decreases as the adsorption site approaches the moiré maximum. A renormalization of the anisotropy has also been observed in model calculations using the one-crossing approximation [32].

Beyond the dramatic variations in line shape with adsorption site relative to the moiré lattice, recorded at the centers of the Fe atoms, we observe remarkable spatial variations also in the immediate vicinity of the adatoms. We illustrate these local variations for Fe atoms located at the minimum of the moiré structure (Fig. 3). (Corresponding data for an Fe atom close to the maximum are shown in the Supplemental Material [19].) At a moiré minimum, spectra recorded directly above the center of the Fe atom show pure inelastic steps. Significant additional structure is observed off center near one of the vertices of the triangle [purple cross in Fig. 3(a)]. Here, the spectrum exhibits substantial bias asymmetry, a conductance overshoot just above the inelastic threshold at positive bias, and an additional dip just below threshold at negative bias [Fig. 3(d)]. We can fit this spectrum within the perturbative approach [26] using the same exchange coupling as for the spectrum taken above the center, but a larger potential scattering amplitude
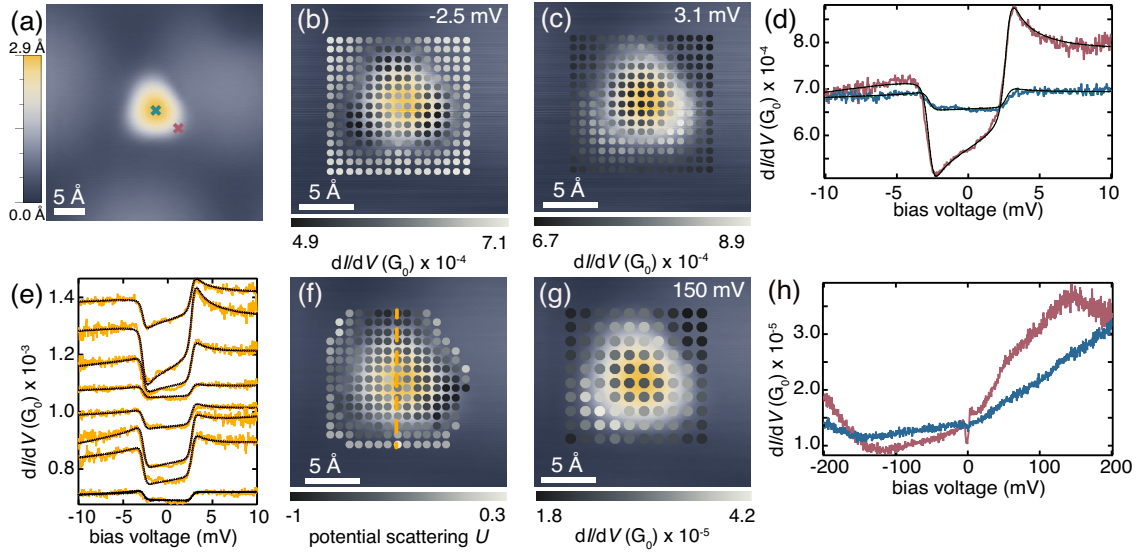
FIG. 3. (a) STM topography of an Fe atom located on a moiré minimum. (b),(c) STM topographies (blue-yellow, background) with superimposed dI/dV signal at the indicated bias voltage (black-white dots, scale below panels) extracted from a densely spaced grid of spectra. (d) dI/dV spectra on the center [indicated by blue cross in (a)] and vertex [indicated with a purple cross in (a)]. Fits (black) as described in [26] with $J\rho = -0.13$, $U = -0.14$, $D = 2.75$ mV (center) and $J\rho = -0.13$, $U = -0.78$, $D = 2.74$ mV (vertex). (e) dI/dV spectra (orange) recorded across the Fe-S complex along the orange line in (f) and fits (black) where $J\rho$ was kept constant in all fits, while U and the transmittivity of the junctions were adjusted. Values of U are shown in the Supplemental Material [19]. Spectra are offset for clarity. (f) STM topography (blue-yellow, background) with superimposed values of the potential scattering parameter U (black-white dots, scale below panel) extracted from fits of a grid of spectra. (g) STM topography with superimposed dI/dV signal at the indicated bias voltage extracted from a grid of spectra. (h) dI/dV spectra over a larger energy range at the same positions as in (b). Spectra in (b)–(f) recorded at $V = 10$ mV, $I = 1$ nA and tip retracted by 20 pm, lock-in frequency $f = 911$ Hz and modulation $V_{rms} = 50\ \mu$V; spectra in (g) and (h) at $V = 10$ mV, $I = 20$ pA and tip retracted by 20 pm, lock-in modulation $V_{rms} = 1$ mV. Grids were analyzed using SpectraFox [33].

U. More generally, all spectra recorded in the immediate vicinity of the Fe atom can be described by adjusting U (as well as the overall tunneling strength) and keeping $J\rho$ constant [see Fig. 3(e) for a set of fits for spectra taken along a high-symmetry axis of the Fe-S complex].

We map out the asymmetry by plotting the dI/dV signal at the energies of the dip and the overshoot [Figs. 3(b) and 3(c)] and the corresponding variations of U obtained from fits of the spectra [Fig. 3(f)]. These maps reveal that the asymmetry is most pronounced at the vertices of the topographic triangular shape. The variations in line shape can be understood as an interference effect [34,35], similar to interference effects underlying asymmetric Fano line shapes of Kondo resonances of magnetic adatoms [36]. In that case, tunneling paths via the adsorbate and directly into the substrate were suggested to interfere [36,37]. Recent works suggest that the interference involves tunneling paths, which are associated with different atomic or molecular orbitals [38–40]. Spatial variations of the asymmetric line shape stem from variations in the tunneling amplitudes via the individual orbitals [41,42].

Our observations can be understood within this latter interpretation. Spectra taken over a wider bias-voltage range [Fig. 3(h)] at the center of the Fe atoms reveal a wide slope across the Fermi level, but are lacking distinct

resonances. In contrast, we observe a resonance at ∼150 mV at the triangle's vertices [for a spatial map see Fig. 3(g)], suggesting the formation of a hybrid Fe-S orbital with weight concentrated on the S atoms. An Fe-S hybrid orbital is consistent with density-functional-theory calculations [24] and explains the triangular shape of the Fe atoms in the STM images.

The nearly symmetric line shape at the center of the Fe-S complex indicates a dominant tunneling path with negligible potential scattering, which is due to cotunneling via the spin-carrying orbitals. The more pronounced bias asymmetry at the vertices originates from cotunneling through an orbital with enhanced potential scattering U. Most likely, this orbital can be identified with the resonance at ∼150 meV as the spatial variations of its map are correlated with the spatial variations of U. The tunneling current at the tip position then depends on the relative contributions of the orbitals in accordance with their spatial structure [42].

Beyond decoupling paramagnetic Fe atoms from the metallic substrate, monolayers of MoS_2 on Au(111) allow for wide tunability of the ratio between the exchange coupling and single-ion anisotropy and thus of the quantum dynamics of the adatom spins. The tuning efficiency is rooted in the moiré modulation of the density of states.

A larger density of states strongly enhances the renormalized exchange coupling and, hence, increases Kondo correlations. Simultaneously, the single-ion anisotropy is reduced. Surprisingly, we observe line shapes ranging all the way from pure inelastic excitations, expected for dominant single-ion anisotropy, to fully developed Kondo resonances, indicating dominant exchange coupling when probing Fe atoms at different locations on the moiré structure. This is complemented by atomic-scale variations of the tunneling line shapes originating from inelastic excitations via different orbitals, reflecting the formation of Fe-S hybrid states. MoS_2 on Au(111) is thus acting not merely as a decoupling layer but rather as a tuning layer for controlling the dynamics of quantum spins, highlighting the potential of interlayers for designing and manipulating quantum spin systems.

---

[*]franke@physik.fu-berlin.de

[1] K. Yang, W. Paul, S.-H. Phark, P. Willke, Y. Bae, T. Choi, T. Esat, A. Ardavan, A. J. Heinrich, and C. P. Lutz, Science **366**, 509 (2019).

[2] P. Willke, W. Paul, F. D. Natterer, K. Yang, Y. Bae, T. Choi, J. Fernández-Rossier, A. J. Heinrich, and C. P. Lutz, Sci. Adv. **4**, eaaq1543 (2018).

[3] A. A. Khajetoorians, S. Lounis, B. Chilian, A. T. Costa, L. Zhou, D. L. Mills, J. Wiebe, and R. Wiesendanger, Phys. Rev. Lett. **106**, 037205 (2011).

[4] A. A. Khajetoorians, T. Schlenk, B. Schweflinghaus, M. dos Santos Dias, M. Steinbrecher, M. Bouhassoune, S. Lounis, J. Wiebe, and R. Wiesendanger, Phys. Rev. Lett. **111**, 157204 (2013).

[5] B. W. Heinrich, L. Braun, J. I. Pascual, and K. J. Franke, Nat. Phys. **9**, 765 (2013).

[6] C. F. Hirjibehedin, C.-Y. Lin, A. F. Otte, M. Ternes, C. P. Lutz, B. A. Jones, and A. J. Heinrich, Science **317**, 1199 (2007).

[7] A. J. Heinrich, J. A. Gupta, C. P. Lutz, and D. M. Eigler, Science **306**, 466 (2004).

[8] S. Loth, M. Etzkorn, C. P. Lutz, D. M. Eigler, and A. J. Heinrich, Science **329**, 1628 (2010).

[9] W. Paul, K. Yang, S. Baumann, N. Romming, T. Choi, C. P. Lutz, and A. J. Heinrich, Nat. Phys. **13**, 403 (2017).

[10] S. Kahle, Z. Deng, N. Malinowski, C. Tonnoir, A. Forment-Aliaga, N. Thontasen, G. Rinke, D. Le, V. Turkowski, T. S. Rahman, S. Rauschenbach, M. Ternes, and K. Kern, Nano Lett. **12**, 518 (2012).

[11] P. Jacobson, T. Herden, M. Muenks, G. Laskin, O. Brovko, V. Stepanyuk, M. Ternes, and K. Kern, Nat. Commun. **6**, 8536 (2015).

[12] F. Donati, Q. Dubout, G. Autès, F. Patthey, F. Calleja, P. Gambardella, O. V. Yazyev, and H. Brune, Phys. Rev. Lett. **111**, 236801 (2013).

[13] Q. Dubout, F. Donati, C. Wäckerlin, F. Calleja, M. Etzkorn, A. Lehnert, L. Claude, P. Gambardella, and H. Brune, Phys. Rev. Lett. **114**, 106807 (2015).

[14] J. Ren, H. Guo, J. Pan, Y. Y. Zhang, X. Wu, H.-G. Luo, S. Du, S. T. Pantelides, and H.-J. Gao, Nano Lett. **14**, 4011 (2014).

[15] N. Krane, C. Lotze, G. Reecht, L. Zhang, A. L. Briseno, and K. J. Franke, ACS Nano **12**, 11698 (2018).

[16] G. Reecht, N. Krane, C. Lotze, L. Zhang, A. L. Briseno, and K. J. Franke, Phys. Rev. Lett. **124**, 116804 (2020).

[17] S. S. Grønborg, S. Ulstrup, M. Bianchi, M. Dendzik, C. E. Sanders, J. V. Lauritsen, P. Hofmann, and J. A. Miwa, Langmuir **31**, 9700 (2015).

[18] N. Krane, C. Lotze, and K. J. Franke, Surf. Sci. **678**, 136 (2018).

[19] See Supplemental Material at http://link.aps.org/supplemental/ 10.1103/PhysRevLett.127.236801 for additional information on (S1) the electronic moiré modulation, (S2) the identification of Fe adatoms on defects, (S3) fit parameters, (S4) determination of the potential scattering U at an Fe atom close to the moiré minimum, (S5) local variations of line shapes on Fe atoms close to the moiré maximum, (S6) interference within a two-orbital model. The Supplemental Material includes Refs. [20,21].

[20] J. Miwa, S. Ulstrup, S. G. Sørensen, M. Dendzik, A. Grubisić Cabo, M. Bianchi, J. V. Lauritsen, and P. Hofmann, Phys. Rev. Lett. **114**, 046802 (2015).

[21] A. Grubisić Cabo, J. A. Miwa, S. S. Grønborg, J. M. Riley, J. C. Johannsen, C. Cacho, O. Alexander, R. T. Chapman, E. Springate, M. Grioni, J. V. Lauritsen, P. D. C. King, P. Hofmann, and S. Ulstrup, Nano Lett. **15**, 5883 (2015).

[22] H. Bana, E. Travaglia, L. Bignardi, P. Lacovig, C. E. Sanders, M. Dendzik, M. Michiardi, M. Bianchi, D. Lizzit, F. Presel, D. D. Angelis, N. Apostol, P. K. Das, J. Fujii, I. Vobornik, R. Larciprete, A. Baraldi, P. Hofmann, and S. Lizzit, 2D Mater. **5**, 035012 (2018).

[23] R. Turanský, K. Palotás, J. Brndiar, Y. J. Li, Y. Sugawara, and I. Stich, Nanotechnology **30**, 095703 (2019).

[24] Y. Wang, B. Wang, R. Huang, B. Gao, F. Kong, and Q. Zhang, Physica (Amsterdam) **63E**, 276 (2014).

[25] X. Chen, L. Zhong, X. Li, and J. Qi, Nanoscale **9**, 2188 (2017).

[26] M. Ternes, New J. Phys. **17**, 063016 (2015).

[27] Density-functional-theory calculations of Fe atoms on free-standing MoS_2 monolayers remain inconclusive regarding the spin state ($S = 1$ or $S = 2$) [24,25].

[28] T. Balashov, T. Schuh, A. F. Takács, A. Ernst, S. Ostanin, J. Henk, I. Mertig, P. Bruno, T. Miyamachi, S. Suga, and W. Wulfhekel, Phys. Rev. Lett. **102**, 257203 (2009).

[29] J. Hermenau, M. Ternes, M. Steinbrecher, R. Wiesendanger, and J. Wiebe, Nano Lett. **18**, 1978 (2018).

[30] P. W. Anderson, J. Phys. C **3**, 2436 (1970).

[31] R. Žitko, R. Peters, and T. Pruschke, Phys. Rev. B **78**, 224404 (2008).

[32] D. Jacob, Phys. Rev. B **97**, 075428 (2018).

[33] M. Ruby, SoftwareX **5**, 31 (2016).

[34] O. Újsághy, J. Kroha, L. Szunyogh, and A. Zawadowski, Phys. Rev. Lett. **85**, 2557 (2000).

[35] A. Schiller and S. Hershfield, Phys. Rev. B **61**, 9036 (2000).

[36] V. Madhavan, W. Chen, T. Jamneala, M. F. Crommie, and N. S. Wingreen, Science **280**, 567 (1998).

[37] M. Ternes, A. J. Heinrich, and W.-D. Schneider, J. Phys. Condens. Matter **21**, 053001 (2009).

[38] S. Frank and D. Jacob, Phys. Rev. B **92**, 235127 (2015).

[39] J. Fernández, P. Roura-Bas, and A. A. Aligia, Phys. Rev. Lett. **126**, 046801 (2021).

[40] M. S. Tacca, T. Jacob, and E. C. Goldberg, Phys. Rev. B **103**, 245419 (2021).

[41] C. Rubio-Verdú, A. Sarasola, D.-J. Choi, Z. Majzik, R. Ebeling, M. R. Calvo, M. M. Ugeda, A. Garcia-Lekue, D. Sánchez-Portal, and J. I. Pascual, Commun. Phys. **1**, 15 (2018).

[42] L. Farinacci, G. Ahmadi, M. Ruby, G. Reecht, B. W. Heinrich, C. Czekelius, F. von Oppen, and K. J. Franke, Phys. Rev. Lett. **125**, 256805 (2020).